J|A|C|S COMMUNICATIONS

Published on Web 07/17/2009

Frustrated Rotations in Single-Molecule Junctions

Young S. Park,[†,§] Jonathan R. Widawsky,[‡,§] Maria Kamenetska,[‡,§] Michael L. Steigerwald,[†] Mark S. Hybertsen,[||] Colin Nuckolls,[†,§] and Latha Venkataraman*[,‡,§]

Department of Chemistry, Department of Applied Physics and Applied Mathematics, and Center for Electron Transport in Molecular Nanostructures, Columbia University, New York, New York, and Center for Functional Nanomaterials, Brookhaven National Laboratories, Upton, New York

Received May 7, 2009; E-mail: lv2117@columbia.edu

Understanding transport through single-molecule junctions is crucial for the development of nanoscale devices.[1] Electron conduction through molecules bonded between metal electrodes depends not only on the molecular structure but also on the metal and the chemical linking group used to bind the molecule to the metal.[2,3] When junctions are formed using gold metal electrodes, thiol links are frequently used.[4,5] However, the conductance of the single-molecule junction varies significantly from junction to junction, making it difficult to map the relation between molecular structure and junction conductance.[6,7] This is in contrast to measurements using amine linking groups[8] for both aliphatic and aromatic compounds[9] and using methyl sulfide and dimethyl phosphines for aliphatic chains.[2] Measurements of single-molecule junctions with thiol links result in a broad distribution of conductances, attributed to different binding geometries at the Au−S bond.[6,7] In particular, the conductance of aromatic molecules is strongly influenced by the orientation of the π system relative to the Au−S bond.[6] While a detailed study of such properties for junctions with thiol links is not possible given the variability in bonding configurations, they can be investigated for junctions with methyl sulfide linkers, where a donor−acceptor bond is formed between an undercoordinated Au atom on the electrode and the S lone pair. Here we compare the conductance of 1,4-bis(methylthio)benzene (**1**) with that of 2,3,6,7-tetrahydrobenzo[1,2-*b*:4,5-*b*′]dithiophene (**3**) and the conductance of 1,4-bis(methylseleno)benzene (**2**) with that of 2,3,6,7-tetrahydrobenzo [1,2-*b*:4,5-*b*′]diselenophene (**4**). Because the orientation of the lone pair is rigidly locked in **3** and **4** but not in **1** and **2** (see the structures in Figure 1B), the results explicitly demonstrate the relationship between the conductance and the orientation of the π system relative to the Au−S or Au−Se donor−acceptor bond.

The syntheses of the molecules are outlined below and described in detail in the Supporting Information (SI). To synthesize **1** or **2**, 1,4-dibromobenzene was dilithiated, and elemental sulfur or selenium was added; the resulting intermediate was then alkylated with methyl iodide.[10] **3** and **4** were synthesized by hydrogenations of the corresponding benzodithiophene and benzodiselenophene, which were performed in the presence of $[Ru(triphos)(MeCN)_3](BPh_4)_2$ at 60 °C.[11]

Single-molecule junctions were created by repeatedly forming and breaking Au point contacts[4] with a modified STM in a solution of the molecules in 1,2,4-trichlorobenzene (Figure 1a). For each molecule studied, the measured conductance traces reveal steps at molecule-dependent conductance values less than the quantum of conductance $G_0 = 2e^2/h$; these are due to conduction through a molecule bonded in the gap between the two Au point contacts (Figure S1). Figure 1b shows conductance histograms generated (without any data selection) from 10 000 consecutively measured traces. We see a peak in the conductance histograms for **3** and **4**

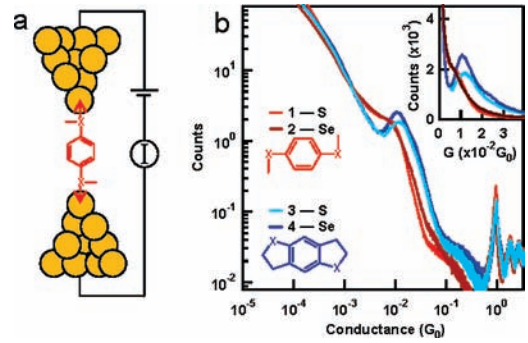

Figure 1. (a) Schematic representation of the measurement. (b) Conductance histograms for the four molecular junctions. Measurements were performed with a 25 mV bias on ∼1 mM solutions of the molecules in 1,2,4-trichlorobenzene. Inset: histograms on a linear scale. The structures of the linkers **1**−**4** are also shown.

when the S (or Se) lone pair is oriented parallel to the π orbital of the phenyl ring. Lorentzian fits to these peaks yield most probable conductance values (defined as the position of the peak) of $(1.20 \pm 0.05) \times 10^{-2}$ and $(1.12 \pm 0.04) \times 10^{-2}$ G_0, respectively. For **1** and **2**, we see a broad increase in histogram counts at a lower conductance range; a Lorentzian (or Gaussian) could not be fit to the data, indicating that there are no dominant conductance values in these measurements (Figure 1b).

In order to understand the difference between these two molecules, we analyzed in detail all of the individual conductance traces used to generate the histograms shown in Figure 1b using an automated algorithm[2] (see the SI). For each conductance trace with a step, we determined the average conductance of the step, the slope of the step normalized to its average conductance, and the step length (Figure S3). We found that for all four molecules studied here, ∼80% of the traces exhibit a step. Figure 2a provides histograms of the average step conductance showing that all of the distributions have clear peaks: $(0.7 \pm 0.05) \times 10^{-2}$ G_0 for **1**, $(0.9 \pm 0.05) \times 10^{-2}$ G_0 for **2**, and $(1.4 \pm 0.05) \times 10^{-2}$ G_0 for **3** and **4**. Analysis of the conductance data based on logarithmic binned histograms also brings out peaks (see Figure S4). These histograms contrast the full-trace histograms shown in Figure 1b and indicate that the junction conductance could change during junction elongation for **1** and **2**, when compared with **3** and **4**. This is further confirmed in Figure 2b, which shows the distribution of normalized step slopes. Although both molecules have sloped steps, a larger fraction of the steps for **1** and **2** are steeper than those for **3** and **4**, as can be seen from the larger full width at half-maximum of the step slope histograms for **1** and **2** than for **3** and **4**.

There are two factors that control the orientation of the S (or Se) lone pair relative to the π system, which in turn controls the measured conductance of these two molecules. First, the probability

[†] Department of Chemistry, Columbia University.
[‡] Department of Applied Physics and Applied Mathematics, Columbia University.
[§] Center for Electron Transport in Molecular Nanostructures, Columbia University.
[||] Brookhaven National Laboratories.

10.1021/ja903731m CCC: $40.75

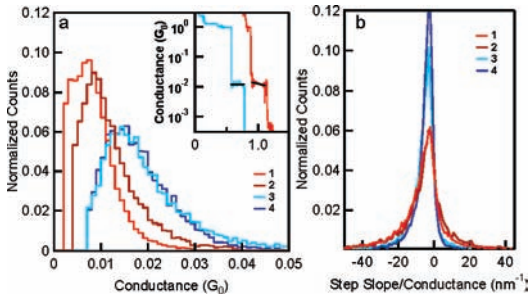

Figure 2. (a) Normalized distributions of average step conductance based on the analysis of 8752, 7415, 21687, and 9256 traces for **1**, **2**, **3**, and **4**, respectively. Inset: Sample conductance traces for **1** and **3** showing a linear fit to the molecular step (black). (b) Distribution of conductance step slope normalized by average step conductance, showing that the conductance steps are more sloped for **1** and **2** than for **3** and **4**, as can be seen from the narrower distribution for **3** and **4**.

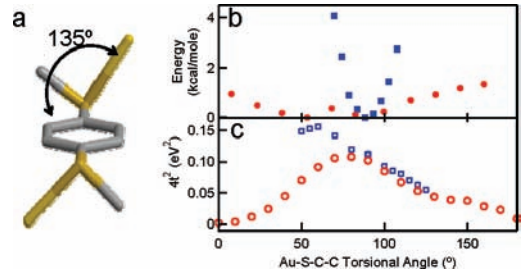

Figure 3. (a) Diagram showing the torsional angle sampled for **1** (see Figure S5 for **3**). (b) Energy as a function of Au−S−C−C torsional angle for **1** (red) and **3** (blue) attached to Au_5 clusters. (c) Square of the calculated tunnel coupling ($4t^2$) across **1** (red) and **3** (blue) attached to Au_1 clusters as a function of the Au−S−C−C torsional angle.

of forming distinct junctions in which the angle between the Au−S link vector and the phenyl plane (Au−S−C−C torsional angle) varies significantly from its minimum-energy configuration in response to other static constraints in the junction contributes directly to the histogram width. Second, the probability of sampling different torsional angles while a specific junction elongates and ultimately breaks affects the measured conductance (thermal average) and the slope of the conductance step. The observed broad histograms for **1** and **2** could thus be explained by the low energy cost for rotating the S (or Se) lone pair away from the π system in the isolated molecule.

To explore this hypothesis more quantitatively, we performed density functional theory (DFT) calculations[12] for **1** and **3** coupled to Au clusters to represent the contacts (see the SI). For both molecules, the Au−S donor−acceptor bond energy ranges from 11 to 14 kcal/mol, depending on the structural details near the Au contact atom. We constrained the natural torsion angle around the S−C bonds in models with an inversion center (equivalent Au−S bonds). The energy cost was evaluated for an Au_5 cluster simulating an Au adatom on the hcp hollow site of an Au(111) facet (Figure S5). As shown in Figure 3b, the torsional energy surface for **1** is very broad, with a barrier to full rotation of ~1 kcal/mol. In contrast, the energy cost to twist **3** is much higher. The tunnel coupling through the junction was probed using Au_1 clusters. The frontier orbitals, of predominantly of Au s/S lone pair antibonding character, are tunneling-coupled through the molecular backbone, resulting in a symmetric and antisymmetric pair with a splitting of $2t$. Similar calculations for a variety of diamine-linked molecules have shown that measured conductance correlates with the square of the calculated tunnel coupling ($4t^2$).[13] The dependence of the calculated tunnel coupling on torsion is shown in Figure 3C. For **1**, the effect of misalignment to the π system of the ring is strong and relatively symmetric. Increasing the torsion for **3** from the minimum-energy configuration results in reduced tunnel coupling, while reducing the torsion initially increases coupling because of buckling of the fivefold ring (Figure S5).

The DFT calculations support a consistent physical picture. For **3**, the high energy cost for torsional angle distortion allows for only an approximately ±15° variation before the junction-formation energy would be too small to sustain a measurement on the millisecond time scale at room temperature. The corresponding variation in the predicted conductance is about ±25%, consistent with a well-defined peak in the histogram in Figure 1B. On the other hand, the flat torsional energy landscape for **1** indicates that as-formed junctions can sample a broad range of tunnel coupling, resulting in a large variation in the measured conductance from junction to junction. Furthermore, a specific junction formed with **1** will thermally access a wide range of angles as well. Therefore, although the nominal tunnel coupling calculated for the minimum-energy geometries of **1** and **3** are similar, the thermally averaged values are rather different. The estimated ratio of the thermally averaged tunnel couplings (1.6) is similar to the ratio of the peak conductance values in the step average histograms of Figure 2A.

In summary, we have established that the orientation of an Au−S or Au−Se bond relative to the aromatic π system controls electron transport through conjugated molecules. In cases such as those discussed herein, the conduction pathway connects the Au electrodes via the chalcogen p lone pairs and the aromatic π system, and greater overlaps among these components leads to higher conductivity through the molecular junction.

Acknowledgment. This work was supported primarily by the NSF-NSEC (Award CHE-0641523), by NYSTAR and the Columbia University RISE program, and in part by the DOE (DE-AC02-98CH10886). L.V. thanks NSF (Career Award CHE-0744185) and the ACS PRF.

Supporting Information Available: Synthesis procedures, data analysis, and theoretical methods. This material is available free of charge via the Internet at http://pubs.acs.org.

References

(1) Joachim, C.; Ratner, M. A. *Proc. Natl. Acad. Sci. U.S.A.* **2005**, *102*, 8800.
(2) Park, Y. S.; Whalley, A.; Kamenetska, M.; Steigerwald, M. L.; Hybertsen, M. S.; Nuckolls, C.; Venkataraman, L. *J. Am. Chem. Soc.* **2007**, *129*, 15768.
(3) Chen, F.; Li, X. L.; Hihath, J.; Huang, Z. F.; Tao, N. J. *J. Am. Chem. Soc.* **2006**, *128*, 15874.
(4) Xu, B. Q.; Tao, N. J. J. *Science* **2003**, *301*, 1221.
(5) Reichert, J.; Ochs, R.; Beckmann, D.; Weber, H. B.; Mayor, M.; von Lohneysen, H. *Phys. Rev. Lett.* **2002**, *88*, 176804. Reed, M. A.; Zhou, C.; Muller, C. J.; Burgin, T. P.; Tour, J. M. *Science* **1997**, *278*, 252.
(6) Basch, H.; Cohen, R.; Ratner, M. A. *Nano Lett.* **2005**, *5*, 1668.
(7) Ulrich, J.; Esrail, D.; Pontius, W.; Venkataraman, L.; Millar, D.; Doerrer, L. H. *J. Phys. Chem. B* **2006**, *110*, 2462. Li, X. L.; He, J.; Hihath, J.; Xu, B. Q.; Lindsay, S. M.; Tao, N. J. *J. Am. Chem. Soc.* **2006**, *128*, 2135. Li, C.; Pobelov, I.; Wandlowski, T.; Bagrets, A.; Arnold, A.; Evers, F. *J. Am. Chem. Soc.* **2008**, *130*, 318. Gonzalez, M. T.; Wu, S. M.; Huber, R.; van der Molen, S. J.; Schonenberger, C.; Calame, M. *Nano Lett.* **2006**, *6*, 2238.
(8) Li, Z.; Kosov, D. S. *Phys. Rev. B* **2007**, *76*, 035415. Quek, S. Y.; Venkataraman, L.; Choi, H. J.; Loule, S. G.; Hybertsen, M. S.; Neaton, J. B. *Nano Lett.* **2007**, *7*, 3477. Kiguchi, M.; Miura, S.; Takahashi, T.; Hara, K.; Sawamura, M.; Murakoshi, K. *J. Phys. Chem. C* **2008**, *112*, 13349.
(9) Venkataraman, L.; Klare, J. E.; Tam, I. W.; Nuckolls, C.; Hybertsen, M. S.; Steigerwald, M. L. *Nano Lett.* **2006**, *6*, 458. Venkataraman, L.; Klare, J. E.; Nuckolls, C.; Hybertsen, M. S.; Steigerwald, M. L. *Nature* **2006**, *442*, 904.
(10) Engman, L.; Hellberg, J. S. E. *J. Organomet. Chem.* **1985**, *296*, 357.
(11) Bianchini, C.; Meli, A.; Moneti, S.; Oberhauser, W.; Vizza, F.; Herrera, V.; Fuentes, A.; Sanchez-Delgado, R. A. *J. Am. Chem. Soc.* **1999**, *121*, 7071. Takimiya, K.; Konda, Y.; Ebata, H.; Niihara, N.; Otsubo, T. *J. Org. Chem.* **2005**, *70*, 10569.
(12) *Jaguar 7.5*; Schrodinger, LLC: New York, 2008. Perdew, J. P.; Burke, K.; Ernzerhof, M. *Phys. Rev. Lett.* **1996**, *77*, 3865. Wadt, W. R.; Hay, P. J. *J. Chem. Phys.* **1985**, *82*, 284.
(13) Hybertsen, M. S.; Venkataraman, L.; Klare, J. E.; Whalley, A. C.; Steigerwald, M. L.; Nuckolls, C. *J. Phys.: Condens. Matter* **2008**, *20*, 374115.

JA903731M